COBEM 2023 27TH INTERNATIONAL CONGRESS OF MECHANICAL ENGENEERING

ABCM Brazilian Society of Mechanical Sciences and Engineering
27th ABCM International Congress of Mechanical Engineering
December 04-08, 2023, Florianópolis-SC, Brazil

EPTT-2022-0186
ESTIMATION OF THE DISSIPATION RATE IN A CENTRIFUGAL PUMP IMPELLER BY USING PIV

William D. P. Fonseca[1‡]
Rodolfo M. Perissinotto [2]
Rafael F. L. Cerqueira [3]
William Monte Verde[2]
Marcelo S. Castro[1,2]
Erick M. Franklin[1]
[1]School of Mechanical Engineering, University of Campinas
[2]Center for Energy and Petroleum Studies, University of Campinas
[3]Mechanical Engineering Department, Federal University of Santa Catarina
[‡]fonsecawdp@gmail.com

Abstract. *The dissipation rate of the turbulent kinetic energy is a key parameter in centrifugal pumps and its local values may have a strong influence on the performance of these devices. Recent technology advancements in particle image velocimetry (PIV) technique have made it possible to study complex turbulent flows at a wide range of scales. In this work, experiments using a time-resolved PIV system were carried out to evaluate characteristics of a turbulent flow, mainly the turbulence dissipation rate, for different operating conditions of a centrifugal pump impeller. In order to overcome the limited spatial resolution constraint, the large-eddy PIV method is used to obtain the dissipation rate. In the large-eddy PIV method, it is assumed that the motion of larger scales is measured by the PIV technique, while the smallest scales (unresolved scales) are modeled by a sub-grid scale model, computed from the strain-rate tensors obtained from the measured fields.*

Keywords: *Turbulent dissipation rate, Centrifugal pump, Particle image velocimetry, Large-eddy PIV*

1. INTRODUCTION

Flow in centrifugal pumps is a constant research topic in fluid dynamics, as these pumps are a widely used in different industrial processes, including agricultural irrigation, water supply, oil facilities, thermal power plants, chemical, nuclear, among others. The internal flow structure in the pump impeller contains high temporal and spatial velocity gradients, vorticity regions, flow separation zones, and intense turbulence levels. Thus, it is important to understand the physics of turbulent flows in these devices, particularly energy transfer from large-scale mean flow to small-scale turbulence and the viscous energy dissipation (Xu and Chen, 2013; Zhang *et al.*, 2018).

In recent studies, experimental techniques with high temporal resolution (e.g. hot-wire anemometry and laser doppler velocimetry) have been used to calculate turbulent characteristics, including turbulent dissipation rate. Following Taylor's frozen flow hypothesis (Hinze, 1975), velocities of temporal fluctuations can be transformed into spatial fluctuations, and the turbulent dissipation rate can be easily calculated, since the spatial velocity gradients are readily available. Nevertheless, these methods cannot provide the global distribution of the dissipation rate over a large flow region.

Contrary to single-point experimental techniques, the particle image velocimetry (PIV) technique can provide instantaneous multi-dimensional (2D or 3D) flow fields. At first glance, the PIV technique seems more suitable for examining the dissipation rate distribution. However, the PIV measured velocity fields have limited spatial resolution, constrained by a combined effect of the tracer particles and the camera sensor size. Therefore, the PIV interrogation windows often exceed the smallest eddy sizes that dominate the turbulence dissipation rate.

In order to obtain dissipation rate with PIV technique, relationships based on isotropy assumptions are proposed in the literature. Sheng *et al.* (2000) employed a large-eddy PIV method to approximate the dissipation of energy at scales below the resolution of the measurements in a stirred tank. The turbulent dissipation rate was estimated from energy flux between the resolved and the sub-grid scales under dynamic equilibrium assumption. The Smagorinsky SGS (sub-grid scale) model (Versteeg and Malalasekera, 2007) was used to estimate the amount of dissipation rate contained in the unresolved scales and at least 70% of the true dissipation was captured. Gabriele *et al.* (2011) used large-eddy PIV to study the effect of particle loading on the modulation of turbulent dissipation rate in a stirred tank. The authors came to the conclusion that large Stokes number particles can suppress turbulence.

Delafosse *et al.* (2011) carried out a study on the influence of the spatial resolution of PIV measurements on the estimated values of the rate of turbulent kinetic energy dissipation. In this study, a total of 12 spatial resolutions were

tested. The authors verified that if the spatial resolution is divided by a factor 2, the dissipation rate increases by 220%. For the smallest spatial resolution value used by the authors, the maximum dissipation rate estimated is 50 times higher than the mean overall rate. Ertürk *et al.* (2013) performed PIV measurements on an external gear pump to also assess the influence of spatial resolution on dissipation rate. Results showed that the spatial resolution is a critical factor in the accuracy of the measurements in the dissipation rate estimations. The optimal results were achieved when the spatial resolution is neither too large (by the sampling phenomenon) nor too small (noise in the measurement data).

Comparisons using different methods to estimate the viscous dissipation rate in turbulent flows were also performed over the years. Gabriele *et al.* (2009) studied the local specific energy dissipation rates in a stirred tank with up- or down-pumping pitched blade turbine with PIV. Three methodologies, direct calculation from fluctuating velocity gradients, dimensional analysis and Smagorinsky closure method to model unresolved length scales, were compared to estimate the local dissipation rate of specific energy. It was found that values from direct calculation method gave 20% of the total value whilst the dimensional analysis and Smagorinsky model methods overestimated it respectively by a factor of 5 and 2. Hoque *et al.* (2015) also compared different methods of estimating energy dissipation rate. The method of direct computation from fluctuating velocity gradients was found to under predict dissipation significantly due to the absence of spatial resolution of velocity gradient. To conclude, according to Hoque *et al.* (2015) spatial resolution is a critical factor in the accuracy of the direct calculation of dissipation rate.

The present work aims the analysis of the turbulent flow in a centrifugal pump impeller, focusing on the measurement of the dissipation of turbulent kinetic energy. For this, experiments using real-time PIV for different pump operating conditions were carried out. It should be noted that the dissipation rate of turbulent kinetic energy is directly related to the performance of the pump, making such analyzes extremely important.

2. EXPERIMENTAL FACILITY

To obtain the velocity data, a centrifugal pump was designed and built out of a transparent material for flow visualization purposes (Fig. 1a and 1b). The impeller has a radial geometry with seven channels of constant height and a small aspect ratio (about $h/D \approx 5\%$) to reduce the three-dimensional flow effects. The impeller outer radius is 55 mm and the inner radius is 22 mm. The volute spiral has a maximum radius of 32 mm. The pump was installed in a hydraulic circuit with instruments to measure pressure, temperature and flow rate.

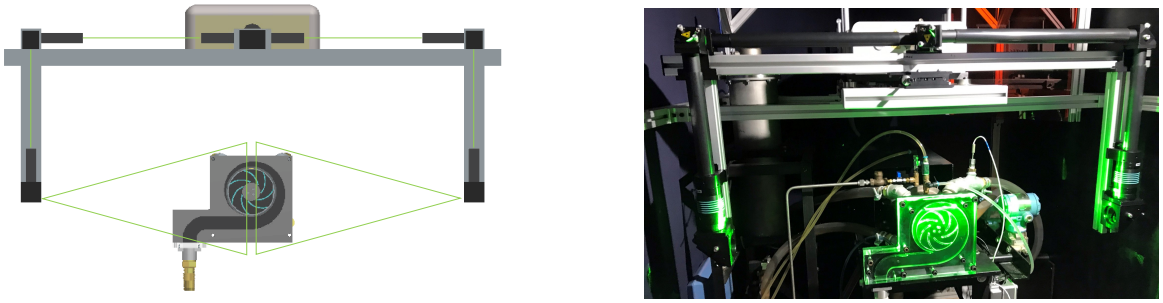

(a) Illustrative scheme of experimental facility (b) Photograph of the experimental facility

Figure 1: Experimental facility with focus on the PIV system and centrifugal pump prototype.

A 2D2C-PIV *DualPower 30-1000* time-resolved system from Dantec Dynamics Inc. obtained the velocity fields within the centrifugal pump. The main components of the system are a laser, a high-speed camera (*Phantom VEO640*) and the DynamicStudio® software, used to control PIV measurements and obtain instantaneous velocity fields. Water was used as the working fluid. Fluorescent particles of PMMA doped with rhodamine B and average diameter of 50 μm were added to the water to serve as tracers. The pump prototype is illuminated from both sides by a dual light guide system composed of beam splitters, mirrors, and light-sheet optics. A high band-pass filter for the wave lengths above 545 nm is mounted on the camera lens, filtering all the light scattered by the interfaces and capturing the light fluoresced by the seeding particles.

The PIV data were acquired during TR-PIV experiments with an acquisition frequency (temporal resolution) of f_{RT-PIV} = 700 Hz. In these experiments, a total of 6,000 PIV frames were recorded. The velocity vectors were estimated using the PIV adaptive method (Scarano and Riethmuller, 1999) with initial and final interrogation regions of 64 and 32 px, respectively. The images were acquired in a double-frame configuration, with a temporal spacing of ΔT=600μs between each frame. This value limited the maximum displacement of the tracer particles to 8 pixels between two consecutive frames, following the guidelines discussed in Raffel *et al.* (2007). In addition, a procedure to remove the angular displacement of the impeller (in order to define a rotating frame of reference) was implemented based on the work of Liu *et al.* (2021). In the present work, the PIV acquisitions were performed at a fixed pump rotational speed of 600 rpm, while the water flow rate was varied at 0.5Q_{BEP}, 1.0Q_{BEP} and 1.5Q_{BEP}, where Q_{BEP} = 1.5 m^3/h is the pump's

Best Efficiency Point (BEP). The rotational Reynolds number $Re = (\omega D)/\nu$ was of the order of 6.9×10^6.

From the pre-defined temporal resolution, the impeller could complete a full revolution after 49 frames. However, since the impeller has an angular symmetry of 51 degrees (i.e., 360° divided by 7 blades), it was considered that the flow in the pump impeller channels completed a full cycle after 7 frames. Since a rotary encoder is mounted on the pump shaft and synchronized with the PIV system, it was possible to average the flow field at a pre-defined rotational angle.

3. ESTIMATION OF TURBULENT DISSIPATION RATE

The turbulent kinetic energy equation for constant viscosity and density can be written as:

$$\frac{\bar{D}k}{\bar{D}t} = \frac{\partial}{\partial x_j}\left[-\frac{\langle u_j p'\rangle}{\rho} + 2\nu\langle u_i s_{ij}\rangle - \frac{1}{2}\langle u_i u_j u_j\rangle\right] - 2\nu\langle s_{ij}s_{ij}\rangle - \langle u_i u_j\rangle \bar{S}_{ij} \tag{1}$$

where the term on the left is the substantial mean derivative of the turbulent kinetic energy k (Eq. 2). The first term in the right-hand side is the transport of turbulence kinetic energy by pressure, viscous stresses and Reynolds stresses, respectively. The second term is the rate of dissipation of turbulence kinetic energy and the last term is turbulence production.

$$k = \frac{1}{2}\langle u_i u_i\rangle \tag{2}$$

The dissipation rate of turbulent kinetic energy can be defined from the Reynolds-averaged turbulent kinetic energy equation. Following Wang *et al.* (2021), the turbulent dissipation rate is derived from the velocity fluctuations gradients as:

$$\varepsilon \approx -2\left\langle \tau_{ij}\bar{S}_{ij}\right\rangle \tag{3}$$

where $\bar{S}_{ij}$ is the strain rate tensor defined by:

$$\bar{S}_{ij} = \frac{1}{2}\left(\frac{\partial\langle U_j\rangle}{\partial x_i} + \frac{\partial\langle U_i\rangle}{\partial x_j}\right) \tag{4}$$

In the equations above, $\langle U\rangle$ represents the mean-flow velocity, u and p' are respectively the velocity and pressure fluctuations, ν the kinetic viscosity and τ_{ij} the stress tensor.

The calculation of turbulent dissipation rate from PIV measurements is limited by the interrogation window sizes, which generally exceed the smallest scales of turbulence. In order to overcome these limitation, Sheng *et al.* (2000) suggests using "large-eddy" ideas from the large eddies simulation (LES). For high Reynolds number flows, the turbulent kinetic energy is generated at large scales and the small-scales structures dissipate the energy provided by larger eddies (Pope, 2000). When a dynamic equilibrium between the energy transferred from largest scales to smallest scales is achieved, the turbulent dissipation rate can be estimated from the flux of turbulent kinetic energy through the inertial sub-range (Ducci and Yianneskis, 2005). Based on this physical model, only the length scales within the inertial sub-range are needed to estimate the flux of turbulent kinetic energy. Thus, the large-eddy PIV method proposed by Sheng *et al.* (2000) does not require the velocity field to be resolved down to the Kolmogorov scale.

Using the Smagorinsky sub-grid model (Smagorinsky, 1963) we can model the stress tensor shown in Eq. (3) as:

$$\tau_{ij} = -C_s^2\Delta^2|\bar{S}|\bar{S}_{ij} \tag{5}$$

where C_s = 0.17 is the Smagorinsky constant. Δ = 3 mm is the average filter width (equal to the interrogation window size), and $\left(C_S^2\Delta^2|\bar{S}|\right)$ is the eddy viscosity, where $|\bar{S}|$ is the filtered rate of strain $|\bar{S}| = \left(2\bar{S}_{ij}\bar{S}_{ij}\right)^{1/2}$. To estimate the dissipation rate from PIV measurements using the large-eddy PIV method, it was evaluated whether the dynamic equilibrium premise is valid. The Kolmogorov length scale (η), estimated from the Reynolds number $\eta = D/Re^{3/4}$, is 0.8 μm. Hence the resolved scale (Δ) is much larger than the Kolmogorov length scale. This clearly calls for the large eddy PIV approach.

In Cartesian co-ordinates ε can be calculated from filtered gradients obtained from 2D-PIV. By assuming isotropic flow to compensate for the unknown z component,

$$\varepsilon = (C_s\Delta)^2\left\{2\left\langle\left(\frac{\partial U_i}{\partial x_i}\right)^2\right\rangle + \left\langle\left(\frac{\partial U_j}{\partial x_i}\right)^2\right\rangle + \left\langle\left(\frac{\partial U_i}{\partial x_j}\right)^2\right\rangle + 2\left\langle\left(\frac{\partial U_j}{\partial x_j}\right)^2\right\rangle + 2\left[\left\langle\left(\frac{\partial U_i}{\partial x_j}\right)\left(\frac{\partial U_j}{\partial x_i}\right)\right\rangle\right]\right\}^{3/2} \tag{6}$$

4. RESULTS

The results shown in this section were acquired with the phase-ensemble averaged fields in the pump impeller, where the impeller is at a rotational angle for θ_{blades} = 0.0 degrees, defined as the angular position where the blade tip is aligned with the volute tongue.

4.1 Phase-ensemble averaged velocity

The phase-ensemble averaged velocity fields under the different flow rates ($0.5Q_{BEP}$, $1.0Q_{BEP}$ and $1.5Q_{BEP}$) are shown in Fig. 2. As can be seen, in the range of the BEP ($1.0Q_{BEP}$), velocity vectors follow the geometry of the blades without significant flow separation. As the flow rate decreases to $0.5Q_{BEP}$, the flow tends to have re-circulation zones, making it unstable. This is associated with the secondary flows of the boundary layer caused by flow transition from pressure blade to suction blade and apparent forces (our frame of reference is non-inertial). In addition, for the flow rate higher than the BEP ($1.5Q_{BEP}$), there are vectors with intense velocities on the pressure blades and the formation of small flow instabilities on the suction blades, which may be associated with the detachment of the boundary layer caused by an adverse pressure gradient (in addition to apparent forces).

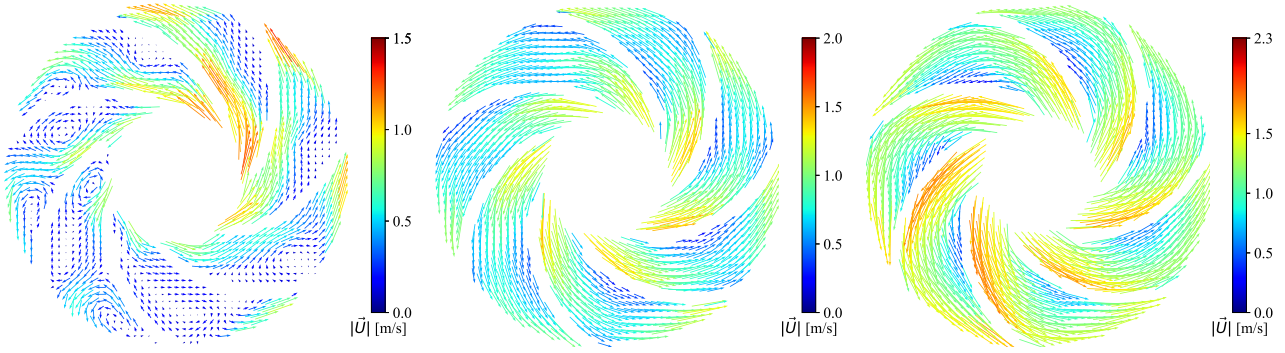

(a) $0.5Q_{BEP}$ (b) $1.0Q_{BEP}$ (c) $1.5Q_{BEP}$

Figure 2: Average velocity distribution in the centrifugal pump impeller.

4.2 Turbulent kinetic energy

The results for the turbulent kinetic energy, defined by Eq. (2), are presented in Fig. 3, and they show that the highest turbulence values are detected at the low flow rate condition ($0.5Q_{BEP}$), especially near the impeller exit. This is because when the fluid flows through the impeller, not only rotational energy is provided to it, but also the volute itself imposes a geometric restriction. As noticed, the highest values of turbulent kinetic energy are located at the leftmost impeller channels, located close to sections where the volute radius is small, while exiting the impeller, the fluid impinges the volute wall, suddenly changing its direction, resulting in the formation of re-circulation zones in the impeller channels. In addition, the flow exiting the impeller in the leftmost bottom channels is affected by the presence of the volute tongue. In this region, as the fluid exits the impeller, it faces a sudden change of direction due to the volute tongue, generating a re-circulation motion. Those two effects combined result in regions with intense local turbulent kinetic energy. On the other hand, for the design ($1.0Q_{BEP}$) and higher flow rate conditions ($1.5Q_{BEP}$), the turbulent kinetic energy presents lower values. This is associated with flow uniformity since the apparent forces present are balanced for such conditions.

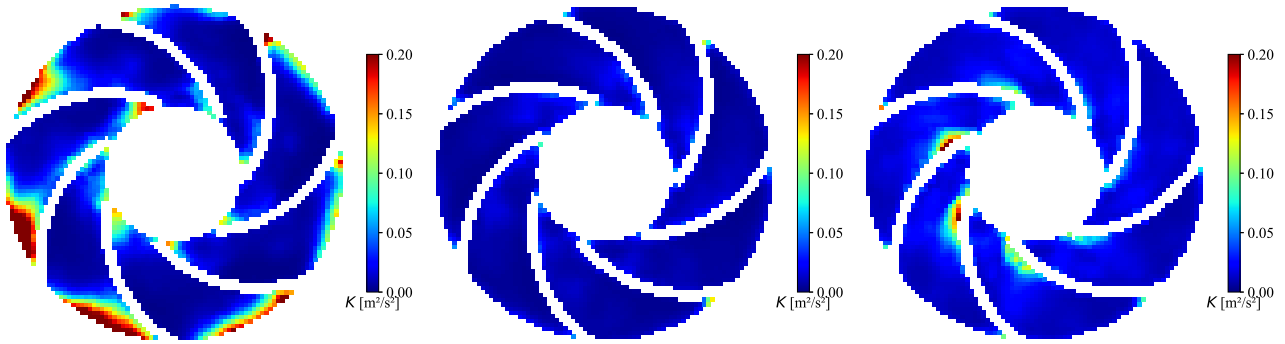

(a) $0.5Q_{BEP}$ (b) $1.0Q_{BEP}$ (c) $1.5Q_{BEP}$

Figure 3: Turbulent kinetic energy distribution in the centrifugal pump impeller.

4.3 Turbulence energy dissipation rate

The turbulent dissipation rate in the centrifugal pump impeller was obtained as indicated by Eq. (6). The spatial derivatives present in this equation were computed using central finite differences. In addition, the large-eddy PIV approach, where the SGS stress is obtained from Smagorinsky model, is used.

As indicated in Fig. 4a, regions of high energy dissipation can be observed for the low flow rate condition, $0.3Q_{BEP}$. It is interesting to note that such regions correspond to the location of high vorticity in the impeller (Fig. 2a), which is an indication that part of the energy generated in this condition is dissipated in this pump component.

For the design and high flow rate conditions, much smaller values of turbulent kinetic energy dissipation are observed. These results indicate that due to the absence of vortical structures in the flow, there is less turbulence production, and as a consequence of the dynamic equilibrium consideration, less energy is dissipated under these centrifugal pump operating conditions.

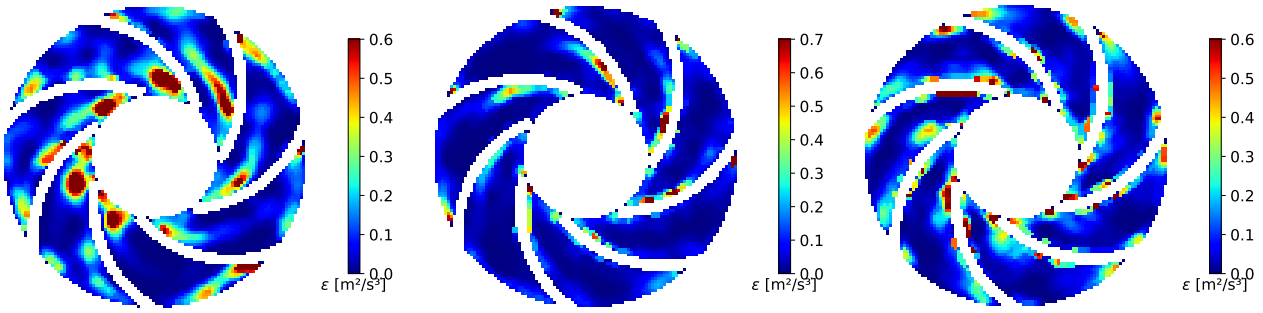

(a) $0.5Q_{BEP}$ (b) $1.0Q_{BEP}$ (c) $1.5Q_{BEP}$

Figure 4: Turbulent dissipation rate distribution in the centrifugal pump impeller.

5. CONCLUSIONS

In this study, we employed PIV measurements to extract qualitative insights into energy dissipation within a centrifugal pump impeller. The large-eddy PIV approach was utilized to calculate the turbulence dissipation. Through a comprehensive analysis of the turbulent flow structure and the distribution of energy dissipation, the following conclusions can be drawn:

1. At the lowest flow rate ($0.3Q_{BEP}$), vortices were observed in channels closer to the volute spiral's tongue, while those farther from it exhibited a different flow topology without such structures. The BEP condition demonstrated a highly organized overall flow. However, at a higher flow rate ($1.5Q_{BEP}$), flow separation occurred at various locations within the impeller, leading to flow instability.

2. For the design ($1.0Q_{BEP}$) and higher flow rate conditions ($1.5Q_{BEP}$), turbulence production exhibited notably low values throughout most regions, except for areas near the impeller inlet. Under part-load conditions ($0.3Q_{BEP}$), localized regions of intense turbulence production were observed near the impeller inlet and outlet.

3. For the low flow rate condition, regions of high energy dissipation correspond to locations of high vorticity in the impeller, suggesting that a portion of the energy generated is dissipated within the pump component. Conversely, the design condition demonstrates considerably smaller values of turbulent dissipation, implying reduced turbulence due to the absence or decreased presence of vortical structures. At the higher flow rate condition, the impeller eye experiences a higher dissipation rate compared to $0.3Q_{BEP}$ and $1.0Q_{BEP}$. Additionally, dissipation is higher on the pressure side of the blades than the suction side, attributed to flow separation predominantly occurring on the pressure side.

6. ACKNOWLEDGEMENTS

We gratefully acknowledge the support of EPIC - Energy Production Innovation Center, hosted by the University of Campinas (UNICAMP) and sponsored by FAPESP – The São Paulo Research Foundation (Process Number 2017/15736-3). We also thank FAPESP for providing the PIV system used in this research through the Multi-User Equipment program (Process Number 2019/20870-6). We acknowledge the support of ANP (Brazil's National Oil, Natural Gas and Biofuels Agency) through the R&D levy regulation. The acknowledgments are also extended to Center for Energy and Petroleum Studies (CEPETRO), School of Mechanical Engineering (FEM), and ALFA Research Group.

7. REFERENCES

Delafosse, A., Collignon, M.L., Crine, M. and Toye, D., 2011. "Estimation of the turbulent kinetic energy dissipation rate from 2d-piv measurements in a vessel stirred by an axial mixel ttp impeller". *Chemical Engineering Science*, Vol. 66, No. 8, pp. 1728–1737.

Ducci, A. and Yianneskis, M., 2005. "Direct determination of energy dissipation in stirred vessels with two-point lda". *AIChE journal*, Vol. 51, No. 8, pp. 2133–2149.

Ertürk, N., Vernet, A., Pallares, J., Castilla, R. and Raush, G., 2013. "Small-scale characteristics and turbulent statistics of the flow in an external gear pump by time-resolved piv". *Flow Measurement and Instrumentation*, Vol. 29, pp. 52–60.

Gabriele, A., Nienow, A. and Simmons, M., 2009. "Use of angle resolved piv to estimate local specific energy dissipation rates for up-and down-pumping pitched blade agitators in a stirred tank". *Chemical Engineering Science*, Vol. 64, No. 1, pp. 126–143.

Gabriele, A., Tsoligkas, A., Kings, I. and Simmons, M., 2011. "Use of piv to measure turbulence modulation in a high throughput stirred vessel with the addition of high stokes number particles for both up-and down-pumping configurations". *Chemical engineering science*, Vol. 66, No. 23, pp. 5862–5874.

Hinze, J.., 1975. *Turbulence*. McGraw-Hill.

Hoque, M.M., Sathe, M.J., Mitra, S., Joshi, J.B. and Evans, G.M., 2015. "Comparison of specific energy dissipation rate calculation methodologies utilising 2d piv velocity measurement". *Chemical Engineering Science*, Vol. 137, pp. 752–767.

Liu, X.D., Liu, Z.Q., Zhong, Q., Li, Y.j. and Yang, W., 2021. "Experimental investigation of relative velocity field based on image rotation method in pump impeller". *Flow Measurement and Instrumentation*, Vol. 82, p. 102061.

Pope, S.B., 2000. *Turbulent flows*. Cambridge university press.

Raffel, M., Willert, C.E., Wereley, S.T. and Kompenhans, J., 2007. *Particle image velocimetry: a practical guide*. Springer.

Scarano, F. and Riethmuller, M.L., 1999. "Iterative multigrid approach in piv image processing with discrete window offset". *Experiments in Fluids*, Vol. 26, No. 6, pp. 513–523.

Sheng, J., Meng, H. and Fox, R., 2000. "A large eddy piv method for turbulence dissipation rate estimation". *Chemical engineering science*, Vol. 55, No. 20, pp. 4423–4434.

Smagorinsky, J., 1963. "General circulation experiments with the primitive equations: I. the basic experiment". *Monthly weather review*, Vol. 91, No. 3, pp. 99–164.

Versteeg, H.K. and Malalasekera, W., 2007. *An introduction to computational fluid dynamics: the finite volume method*. Pearson education.

Wang, G., Yang, F., Wu, K., Ma, Y., Peng, C., Liu, T. and Wang, L.P., 2021. "Estimation of the dissipation rate of turbulent kinetic energy: A review". *Chemical Engineering Science*, Vol. 229, p. 116133.

Xu, D. and Chen, J., 2013. "Accurate estimate of turbulent dissipation rate using piv data". *Experimental Thermal and Fluid Science*, Vol. 44, pp. 662–672.

Zhang, N., Gao, B., Li, Z., Ni, D. and Jiang, Q., 2018. "Unsteady flow structure and its evolution in a low specific speed centrifugal pump measured by piv". *Experimental Thermal and Fluid Science*, Vol. 97, pp. 133–144.

8. RESPONSIBILITY NOTICE

The authors are solely responsible for the printed material included in this paper.